Research Article

Large-Eddy Simulation of the Aerodynamic and Aeroacoustic Performance of a Ventilation Fan

Stefano Bianchi,[1] Domenico Borello,[1] Alessandro Corsini,[1] Franco Rispoli,[1] and Anthony G. Sheard[2]

[1] *Department of Mechanical and Aerospace Engineering, Sapienza, University of Rome, Via Eudossiana, 18, 00184 Roma, Italy*
[2] *Fläkt Woods Ltd., Axial Way, Colchester CO4 5ZG, UK*

Correspondence should be addressed to Alessandro Corsini; corsini@dma.ing.uniroma1.it

There are controversial requirements involved in developing numerical methodologies in order to compute the flow in industrial fans. The full resolution of turbulence spectrum in such high-Reynolds number flow configurations entails unreasonably expensive computational costs. The authors applied the study to a large unidirectional axial flow fan unit for tunnel ventilation to operate in the forward direction under ambient conditions. This delivered cooling air to the tunnel under routine operation, or hot gases at 400°C under emergency conditions in the event of a tunnel fire. The simulations were carried out using the open source code OpenFOAM, within which they implemented a very large eddy simulation (VLES) based on one-equation SGS model to solve a transport equation for the modelled (subgrid) turbulent kinetic energy. This subgrid turbulence model improvement is a remedial strategy in VLES of high-Reynolds number industrial flows which are able to tackle the turbulence spectrum's well-known insufficient resolution. The VLES of the industrial fan permits detecting the unsteady topology of the rotor flow. This paper explores the evolution of secondary flow phenomena and speculates on its influence on the actual load capability when operating at peak-pressure condition. Predicted noise emissions, in terms of sound pressure level spectra, are also compared with experimental results and found to agree within the uncertainty of the measurements.

1. Introduction

The selection of the state-of-the-art industrial fan technologies for tunnel ventilation normally fulfills user demands that require high volume flow rates and total pressure rises. As such, the specified operating area falls in several cases within the range ordinarily characterizing mixed flow fans. In addition to these performance requirements, two additional factors contribute to the complexity of design processes of the fan range customized for emergency and routine operating modes [1, 2]. First, the fan must have installation in either a vertical or horizontal layout and, second, the fan range must be able to accommodate the effect of unsteady pressure pulses which the trains generated in ventilation shafts [3–6].

These requirements imply levels of complexity in the design process and diversity in the operations that are significantly beyond the historic norm within the fan industry. Therefore, the application of standard methodologies is inappropriate and significant changes are taking place in the design process of large industrial fans. Although the conventional approach to fan design has historically involved trial-and-error empirical methods that rely on the designer's experience of aerodynamics [7, 8], more recent approaches to the design of state-of-the-art fan units have utilised computational fluid dynamics (CFD) analyses at the early stage of the process. Amongst others, Vad [9] and Corsini et al. [10] have proposed improved designs. These scholars developed a family of high-performance swept fans for mine ventilation by feeding-back the three-dimensional (3D) design criterion with the computed secondary flow aerodynamics. Lee et al. [11] applied an inverse approach to the design of cooling fans for electronic appliances, which

included the combined use of a "design of experiments" step and CFD to explore the space available for design solutions. In doing so, the above-mentioned scholars transferred design methodologies reliant on CFD to develop appropriate 3D blades [12].

Historically, aerodynamic considerations primarily have constrained large fan designers. Initially, they would produce an aerodynamic design by scaling smaller unit characteristics with the final design's actual performance which the experimental testing established. However, recent legislative developments and standards relating to tunnel ventilation system fans have impacted fan design, resulting in unusual design choices, for example, increased tip gap or solidity and blade thickness which is mechanical rather than aerodynamic implications drive.

It is apparent that the EN 12101-3 and ISO 21927-3 [3, 5] constraints on industrial fan designers are driving continuing market demand for fans that can provide higher performance and less noise. In response to these constraints, industrial fan designers require a methodology that combines finite-element analysis (FEA) (for mechanical analysis) and CFD (for aerodynamic and aeroacoustic analysis) to provide a virtual prototyping design methodology that replaces traditional testing and evaluation methods in fan development. Although virtual-prototyping techniques are presently uncommon in the fan industry, they provide cross-functional evaluations of competing objectives and enable designers to consider "downstream design issues" in the initial stages [13, 14]. The process of virtual prototyping reduces the need to build physical prototypes and facilitates the early identification of design problems, thus reducing product development costs. Sheard et al. [15] case study proposed virtual prototypes to characterize the aerodynamic and acoustic profiles of a new range of large industrial fans.

A key ingredient in buildingup accurate virtual prototype is turbulence computations. U-RANS and hybrid LES/RANS turbulence closure usage allows the simulation only of (part of) the flow unsteadiness without fully accounting for the influence of turbulence spectrum on flow unsteadiness. The proper simulation of the unsteady aerodynamics is also crucial in providing physical insights of the secondary flow structure and in recognizing the major contribution to fan noise emission. On the other hand, proper LES solutions are hardly available in the open literature due to the formidable computational effort required to solve the turbulent spectrum up to the inertial subrange (e.g., Schneider et al. [16]). However, in high-Reynolds number turbomachinery flow VLES with a proper resolution of the larger turbulent scales in the computational domain [17] are inherently unable to solve turbulence scale up to the inertial subrange. In such a condition, the hypothesis of stationary, isotropic vortex cascade does not hold because of the occurrence of localized backscattering phenomena. Consequently an appropriate subgrid scale motion, able to take in account at least backscattering effect, should be considered when VLES computations are performed (e.g., dynamic model of Germano or one-equation subgrid scale model of Davidson and Nielsen [18]).

The majority of the published turbomachinery noise research has been focused on high-speed fans and compressors [19, 20]. Notably, for a number of years, it has been accepted that noise was not of importance even in high bypass ratio fans used in jet engines, where it became dominant only at low power settings [20]. The noise abatement requirements in civil legislation have recently highlighted the importance of industrial fan noise. Consequently industrial fan designers are now interested in tools that will enable them to predict industrial fan noise. The character of fan noise, also in low-speed unit, is similar to compressors in that it consists mostly of tones originating from the multiple blades. The tones radiate through the shear layer between the rotating blades and static vanes. This causes the tones to scatter into adjacent frequency bands and appear as "haystacks" when measured in the far-field. Since there can be many tones, even with narrowband analysis, the tones may appear as broadband noise.

The investigation reported in this paper used a hybrid approach, where the aerodynamic flow-field was numerically characterized, using CFD methods and an associated noise prediction method, based on the formulation by Ffowcs Williams Hawkings equations [21]. The aim of the present work is to develop a fan acoustic prediction tool for the estimation of the noise during the preliminary design phase. The analytic prediction technique is designed to resolve up to the fifth harmonic of the blade passing frequency tone and the goal is to validate the use of aerodynamic calculations to generate the necessary input for the rotor noise prediction model. The noise calculation method models blade and vane interactions, but do not take account of quadrupole sources or duct modes. Because of the preliminary nature of the acoustic prediction method, the rotor noise prediction is limited to a free space application and the duct implementations will be developed in a future program of work.

In recent years, open source philosophy has provided a new impetus in CFD code development. An open source code allows researchers to collaborate in developing fluid-dynamic software with accurate numerical schemes, fast solution algorithms, and a wide selection of flow models. In the present study the authors used the open source code OpenFOAM (http://www.openfoam.com/) [22], already used to carry out Detached-Eddy-Simulation and LES of the industrial fan under scrutiny [23, 24]. The use of U-RANS first order closure, hybrid LES/RANS, and VLES is well established in turbomachinery and industrial flow predictions. Despite contradictory findings, the authors documented noticeable results for both steady and unsteady approaches [25–31].

In this paper, the authors discuss the unsteady aerodynamics of the industrial fan under scrutiny. After the illustration of the flow topology, the study accounts for the evolution of secondary flow phenomena in order to establish the link with the unsteady variation of fan load and losses.

2. Description of the Fan

The range of large industrial fans under scrutiny was designed to comply with the legislative framework embodied in

TABLE 1: Fan range description.

Size range, D_{tip}	1.4 m–2.8 m
Performance standard	ISO 5801
Volume flow rate	$10\,\text{m}^3/\text{s}$–$300\,\text{m}^3/\text{s}$
Total pressure rise	500 Pa–3000 Pa
rpm	900, 1500
High temperature certification	200˚C, 300˚C and 400˚C

TABLE 2: Fan blade data at midspan.

Blade section	ARA-D	
Diameter at the tip (mm)	2240	
Blade count	16	
Hub-to-tip diameter ratio	0.5	
	Hub	Tip
Chord (mm)	143	92.5
Solidity (–)	0.64	0.21
Pitch angle (deg)	48	24

the EN 12101-3 and ISO 21927-3 standards, in force for tunnel ventilation. According to the specifications, relating to the installed fan performance, large fans intended for application in tunnel and metro ventilation systems must operate at elevated temperatures during an emergency whilst meeting specified noise emission requirements (i.e., 80 dBA in emergency and 50 dBA during routine operations). In addition to these requirements for emergency and routine operating modes, the fan must run at different speeds and accommodate the effect of unsteady pressure pulses that trains generate in tunnels when they pass a ventilation shaft.

Table 1 lists the specifications of the fan range. It consisted of seven standard diameters, and the performance requirements span over a range of duties typical of tunnel ventilation systems.

Specifically, the fan under investigation was a 2.24 m diameter unidirectional fan spun by a 4-pole motor at 1500 rpm [15]. Figure 1 shows the 2.24 m prototype fan, labeled 224JFM, with newly designed blades suitable for one-time only emergency operation at 400˚C. Table 2 specifies the geometrical data of the blade of 224JFM fan.

Moreover, Figure 2 describes the operating region of the ventilation fan under scrutiny in terms of the total pressure (Δp_t) to volume flow rate (V) characteristic curves when varying the pitch angle, as measured at the blade tip, from 8 to 24 degrees.

3. Methodology

3.1. Numerical Method. The computational analysis was based on the use of the open source finite volume CFD code OpenFOAM 1.7.x written in C++. The LES prediction of the fluid motion is computed by solving the filtered unsteady Navier-Stokes equations system. The subgrid scales closure is modelled using the local dynamic k-equation model of Ffowks Williams and Hawkings [21], which the authors modified to take in account the occurrence of backscattering

(i.e., kinetic energy transfer from smaller to greater scales), allowing the occurrence of negative subgrid scale viscosity ν_{sgs}.

In the present computations the LES computation is based on a central difference space discretization with an accurate TVD scheme to prevent numerical instabilities and a second-order accurate implicit approach for time marching solution. Concerning the solution strategy, the discretised Navier-Stokes and turbulence equations are solved by adopting an ILU preconditioned semi-iterative conjugate gradient linear solver, in combination with a PISO segregation scheme. To account for the fan rotation, the original segregated solver (PISOFoam) was modified to consider the influence of Coriolis and centrifugal forces in the relative frame of reference.

The nondimensional time step was set equal to 2×10^{-5} to keep the CFL number under the value of 0.7. Starting from a preliminary URANS computed flow field, the LES was performed for 2 flow through time (FTT) before acquiring flow field data. All the results in the next sections have been computed by collecting statistics during 1.5 FTT corresponding to 54 blade revolutions.

3.2. Aeroacoustic Method. The method applied in this paper has been programmed in Matlab. Once the experimental data is loaded the time resolved formulation of Lighthill's acoustic analogy is used [32]. The formulation consists of FW-H equations and Farassat solutions for rotating surfaces [33].

The present work used a specific procedure to interpolate the source terms from the computational results and to compute the noise radiation. Virtual pressure transducers located on the blades proximity with regular chord-wise and span-wise spacing give the near field sources. The pressure fluctuations were derived from the LES and phase-locked averaged to obtain the unsteady pressure data. The time-resolved pressure fluctuation data were used in order to calculate the fundamental quantities requested by the Farassat formulation of acoustic analogy. The virtual probes matrix on the blades surface represented the aerodynamic mesh. Each probe contributes to the calculation of the local Mach numbers and the fluctuating lift force on the blades, which fed the model at each temporal step.

The method is a two-step hybrid approach relying on Lighthill's acoustic analogy [32], which assumes the decoupling of noise generation and propagation. The first step consists on recording the noise source in the aerodynamic domain as computed during the computational campaign. In the second step, a variation of Lighthill's acoustic analogy is solved in the time domain, resulting in a calculation of the radiated tonal noise into the free-field. As a consequence of the use of a modified Farassat solution [33] of the Ffowcs Williams Hawkings equation [21], it is possible to take into account the subsonic sources present in a fan discharged flow. The approximation for the noise source used in this work, based on a truncated form of the Farassat solution and integrated on the collapsing sphere [33], is valid for an observer position in the rotor plane. To accomplish this condition, the observer position was localized in the plane

(a)   (b)
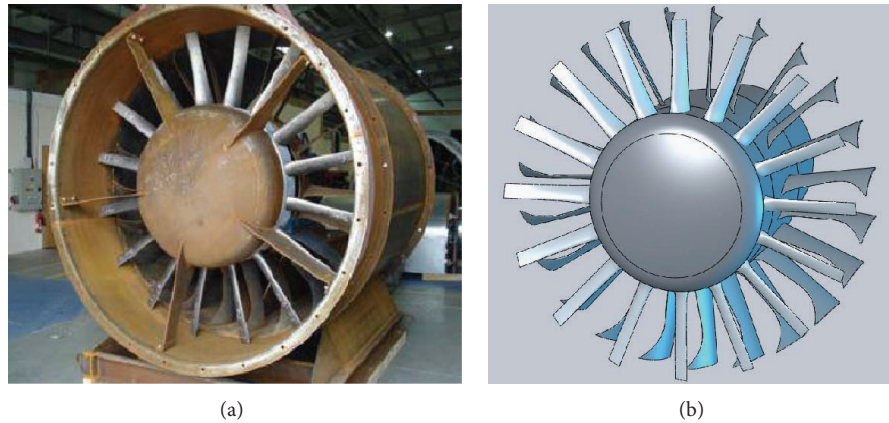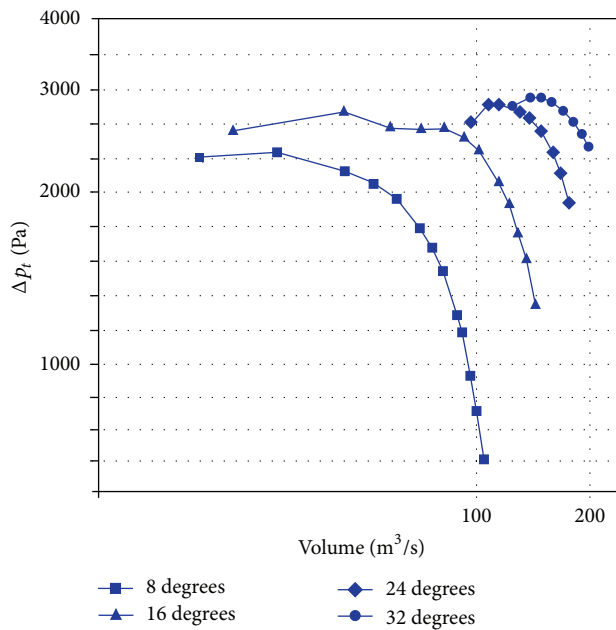
FIGURE 1: Fan 224JFM.

FIGURE 2: Total pressure volume operating margin 224JFM.

of rotation on a side of the rotor. The present method was previously validated by the authors in an acoustic study of tonal noise in a transonic rotor [34], which provides the analytical details of the proposed technique. From an algorithmic viewpoint, the model is structured according to the ensuing passages: (i) time history of the source terms is stored in the results file; (ii) an acoustic coarse mesh is built around the whole region of interest including the domain where aeroacoustic sources are present; (iii) source terms are interpolated on the coarser acoustic mesh; (iv) acoustic computation is performed taking into account the spectral volume source terms.

The acoustic signature of the rotor is derived by shifting the signature of one blade in time by the number of blades and summing the pressures for each observer time within a period, based on the blade passing frequency. One limitation

assumed by the authors in this preliminary model was to neglect the duct cut-off effect of the spinning off modes. In the model the authors used, the observer is considered in the plane of rotation, thus normal to the fan axis. The free field approximation is then reliable only for the frequency location of the tones.

3.3. Numerical Grid and Boundary Conditions. The authors conducted the test using a 24 deg pitch angle setting. The Reynolds number, based on tip diameter and rotor tip speed, is 8.7×10^{6}. In all the numerical campaigns, normal air condition was assumed. The computational domain, which Figure 3 illustrates, extends half chord upstream of the leading edge and one chord downstream from the trailing edge.

The mesh was built according to a nonorthogonal body fitted coordinate system with an immersed blade, using a block-structured topology. The mesh consisted of about 9×10^{6} nodes and 8.8×10^{6} hexahedral cells. Table 3 provides details of the rotor grid. Concerning the distribution of the elements in the axial direction, it consists of 16%, 50% and 34% of nodes respectively upstream of the leading edge, in the blade passage and downstream from it. Moreover, 55 cells are used to model the tip-clearance along the span. The mesh has an adequate clustering toward solid boundaries, with the ratio of minimum grid spacing on solid walls to mid-span blade chord set as 7×10^{-4} on the blade tip, casing wall, and blade surfaces. The adopted grid refinement towards the solid surfaces controls the normalised wall distance $y+$ value about 1 on the first nodes row.

The inflow boundary conditions were set to account for the distortion effects induced by the spinner cone upstream the rotor leading edge [15]. Flow periodicity, upstream, and downstream of the blade row, and Neumann outflow conditions complete the set of boundary data. Notably, whilst a steady velocity profile is imposed at the inlet, the flow unsteadiness develops within the rotor blading under the forcing influence of strong vortical structures generated on the endwalls.
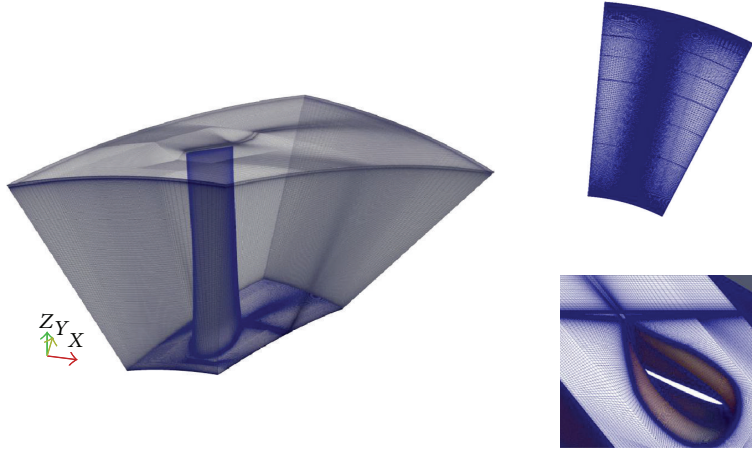
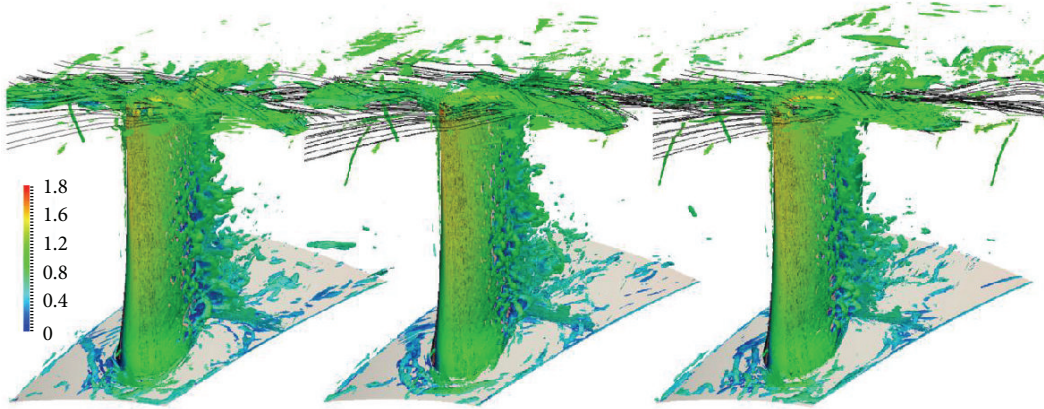FIGURE 3: Computational domain and details of the grid.

FIGURE 4: Flow topology $\nabla^2 p = 1000$ isosurfaces coloured with velocity magnitude.

TABLE 3: Fan mesh data.

	Rotor
Nodes	9,021,968
Cells	8,862,550
Tip gap nodes	60,753
Tip gap cells	52,000
Blade surface cells	62,450
Averaged cell aspect ratio	1.34

4. Results

The analysis of the unsteady aerodynamic of the fan is carried out with an angular setting of 24 deg in proximity of the peak-pressure operation close to the rotating stall incipience. In this condition, the fan delivers $120\,\mathrm{m}^3/\mathrm{s}$ with a total pressure rise of 2806 Pa. The investigation, first, focused on the reconstruction of the three-dimensional flow topology in the blade vane with emphasis on the secondary flow phenomena. Then, the authors speculated on the unsteady evolution of the load along the blade span when approaching the peak pressure limiting operation.

4.1. Flow Topology. The authors discuss, first, the flow topology as per the evolution in time of the major vortical flow structures when the fan is operated close to its pressure limit. The vortex eduction analysis was, therefore, carried out by the prediction of the pressure Laplacian $\nabla^2 p$ isosurfaces. This scalar quantity, which correlates to the well-known Q criterion, identifies coherent vortices in separated flows and was found to be more informative in case of flows bounded by compact walls [35].

The discussion of the flow topology is carried out using the method of Dubief and Delcayre [35] by plotting the evolution of instantaneous $\nabla^2 p$ isosurfaces around the fan blade. Figure 4 shows a perspective view of the blade stacking at three instants with a constant time interval equivalent to 0.3 normalized time. In particular, Figure 4 illustrates the 3D view of the $\nabla^2 p = 1000$ isosurfaces coloured by the relative velocity magnitude.

As expected, vortical structures are generated though the lack of any unsteadiness at the inflow. The onset of vortical and secondary flow structures mostly correlated to the aerodynamic interaction between the incoming flow and the blade which develops along the span with dramatic thickness
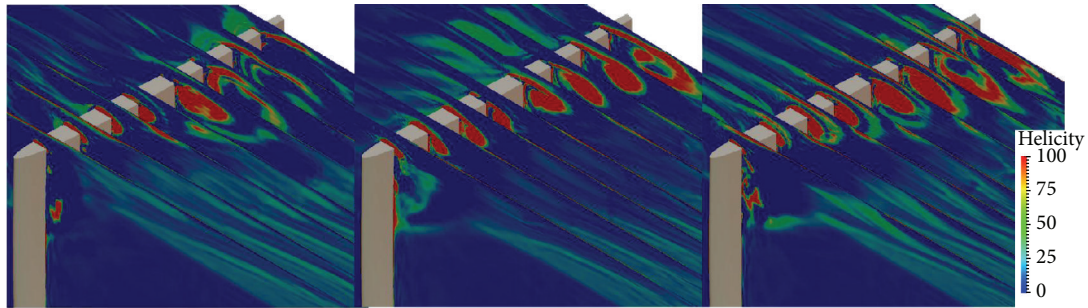
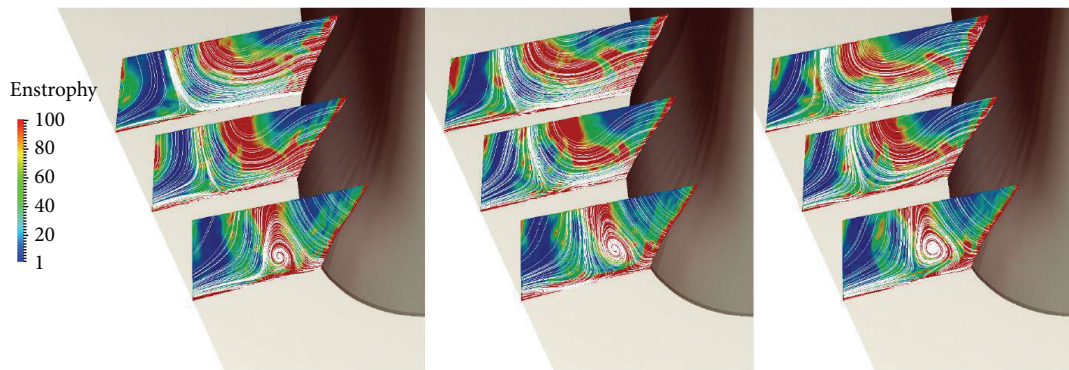FIGURE 5: Tip leakage vortices eduction by the helicity contours.

FIGURE 6: Horse-shoe vortex visualization by enstrophy contours and streamlines.

variation as per the mechanical design requirements under the 400°C specification.

On the hub the local bluntness of the blade resulted in a typical horse shoe vortex like structure whose suction and pressure side legs clearly marked the collateral boundary layer deviation about the leading edge. Moreover, the generation of a system of horseshoe vortices is evident including a smaller one close to the leading edge, and a second bigger one with a wider opening angle is present slightly upstream. As given by the time evolution in **Figure** 4, the horse-shoe vortex appeared to stably influence the inner endwall. Whilst the chordwise pressure field immediately strained the suction side leg, the pressure side one was found to have a longer streamwise evolution.

When looking at midspan, notably the shedding of vortical structures in the wake still develops under the influence of the aerodynamical design in the inner portion of the blade which was thickened due to structural reasons. This influence and the correlated intensity of the vortex shedding, gradually decreased when moving above midspan.

Finally, approaching the outer endwall, **Figure** 4 demonstrates that near the casing the tip leakage vortex represents the most relevant structure. Here, once again, the main tip leakage vortical formation moving across the blade vane at the leading edge developed stably while set of the tip leakage vortices, close to the blade surface, suffered an evident time dependence. Notably, the location of the larger tip leakage vortex was in accord with the actual operation in a prestall

condition which is frequently correlated with a leakage vortex spillage.

In order to provide additional hints on the time evolution of those secondary phenomena found in the rotor flow topology, **Figure** 5 shows the contours of the helicity at the blade tip at three time abscissa again collected at constant time interval equivalent to 0.3 normalized time.

Figure 5 gave a clear evidence of the multiple vortex behaviour which featured the fan under investigation according to the enlarged tip gap which resulted from the high temperature classification requirements. This geometrical element played a critical aerodynamic role and reflected in the large unsteadiness found in the time evolution of the swirling core at the blade tip. When comparing the helicity patterns, it was apparent that whilst the onset of the vortices stayed constantly in proximity of the blade leading edge, the swirling flow dynamics resulted in a periodical variation of the helicity level at the blade trailing edge.

To illustrate the evolution of the pressure side leg of the horse-shoe vortex at the hub, moreover, **Figure** 6 shows the contours of the enstrophy (which is defined as the integral of the square vorticity) at different axial section along the blade surface. The authors plotted the enstrophy contours on each section against the streamlines. Notably, when compared to the structures at the tip, the horse shoe vortex appeared to be stable. This circumstance is an indirect evidence of the origin of this peculiar vortical structure dictated by the geometry of the leading edge at the blade hub section.
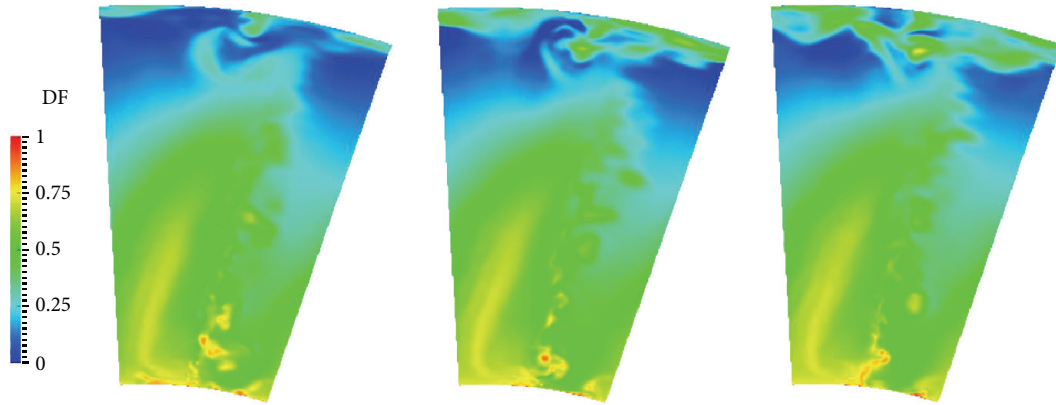
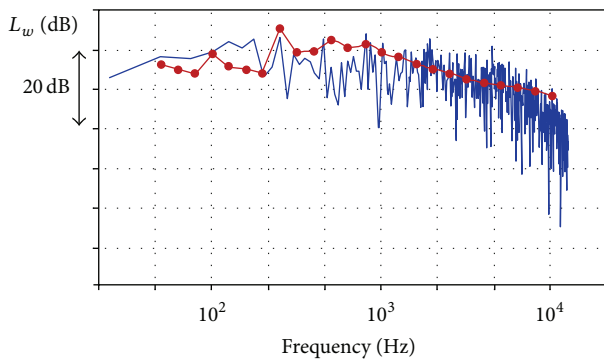Figure 7: Diffusion factor DF evolution behind the rotor.

Figure 8: Comparison of sound power level spectra at design condition (line-symbol: experiments; line: computation).

4.2. Unsteady Load Analysis. A further step in the investigation was to quantify the influence of the aerodynamic unsteadiness on the work capability of the rotor. To this end, Figure 7 shows the distribution of the local diffusion factor (DF) computed according to the Lieblein definition [36].

Figure 7 compares the evolution of DF behind the fan rotor by plotting the contours at three time abscissae taken at constant time interval 0.3 normalized time long.

As expected the secondary flow structure affected the load condition along the blade span. In accordance with the flow topology findings, at the blade hub the deviation of the flow was influenced by the shedding of vortical structures. In particular, on the suction side the wake distorted steadily the DF distribution whilst on the pressure side of the blade, it was possible to find a large unsteadiness as the result of the stronger horse-shoe vortex leg.

At the tip, where according to the prescribed radial work distribution the rotor is unloaded, the tip vortices produced large fluctuations in the local blade deviation and deceleration capability. Notably, this unsteady behaviour occurred at peak pressure condition with the rotor close to a prestall operation.

4.3. Aeroacoustic Analysis. Figure 8 plots the sound power level L_W (dB) spectrum measured in-duct [37] against the spectrum computed by using the FW-H method at design conditions.

Notably, the FFT, normalised in dB acoustic response (reference pressure of $20\,\mu$Pa), is calculated for the overall noise pressure signal at the observer position. The timescale of the signal was associated to the rotor rotation. For a sensor in the absolute frame time is made dimensionless with the rotor-passing period. By contrast the time axis of the fluctuations measured by gauges located on the rotor are made dimensionless with the stator-passing period.

Figure 8 demonstrates the fair agreement of the predicted spectrum with the experimental data. Although the model is shown to overpredict the low frequency range, the matching is worthy of note at the first blade passing frequency and over the range of the tonal sources up to the third harmonic. An underprediction of the model characterised the blade passing frequency harmonics intertonal spectrum. Focusing on broadband noise, after $f = 1$ kHz the broadband noise amplitude oscillated around the experimental value and then was under predicted after $f = 7$ kHz. This behaviour may be as a consequence of the limits of the adopted model, as the model neglects duct modes. Consequently the model may miss the modal amplification of the dipole-like noise sources, characteristic of intertonal, and broadband noise, when compared with an in duct acoustic measurements.

In order to provide insight into the blade sound sources, Figure 9 shows their distribution and evolution in time. In particular the quality of the sound origin about the blade is illustrated by using the aerodynamic source term calculated according to the Powell's theory [38]. Powell observed that the fluctuating pressure exerted upon a rigid boundary by a contiguous unsteady flow can be shown in a formal manner to generate sound as of a distribution of dipoles. It can be argued, by means of the reflection principle, that all such dipole effects cancel out due to the interaction of modes and duct reflection modes. Past studies [39] confirm the presence of effective dipole-like generators when a fluctuating pressure is exerted on a rigid boundary. The Powell's vortex sound theory directly models the aerodynamic aspects of the aerodynamic sound generation and may be written as follows:

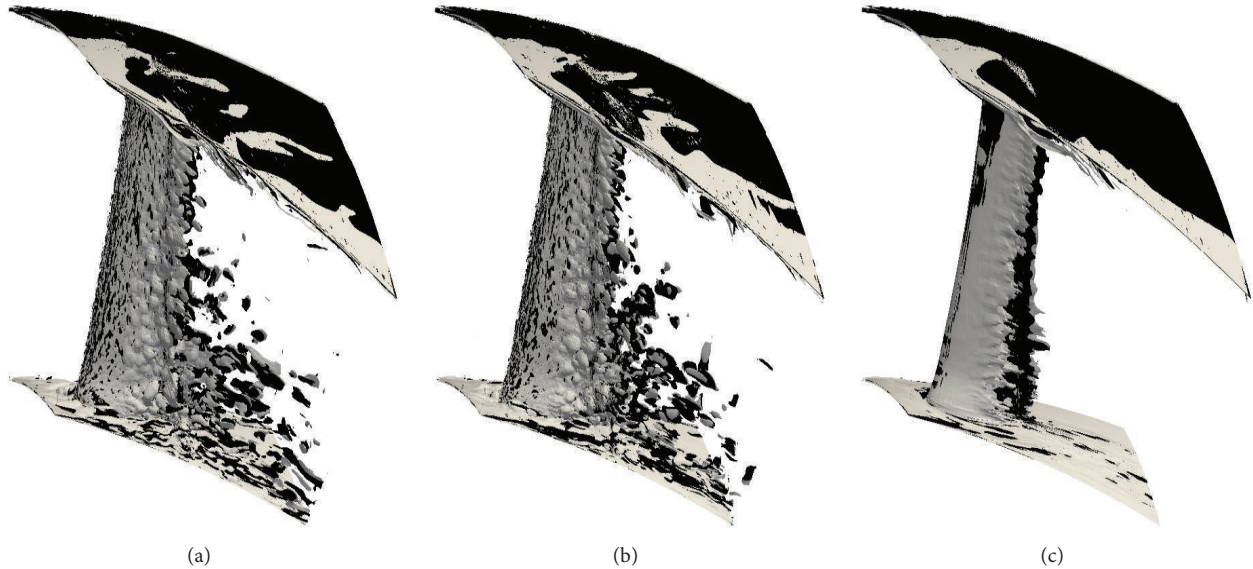$$\nabla \cdot (\omega \times v), \tag{1}$$

(a)

(b)

(c)

Figure 9: Powell's sound source distribution in two different time steps (at a distance of 0.5 FTT) and time averaged value (right).

where, as in Powell [40], the source terms depend on ω (the vortex vector of the leakage flow) and ν (its convection velocity).

Figure 9 illustrates the Powell's sound sources by plotting the instantaneous isosurfaces against the time averaged one. The more active aerodynamic sound sources located just behind the trailing edge are those linked with the fluctuations of vorticity in the wake. In the wake region, the alternating vortices come from both sides of the airfoil, and this vortex motion stretches the separated shear layer. The separated shear layer therefore rolls up at this region, with the consequent production of noise. Because the structure of the wake is unstable, the sound source changes in the time domain. If the source term has a high velocity ratio, the sound source term has a two-dimensional structure.

At the blade tip, Figure 9 shows also the isosurface of the sound sources correlated with the tip leakage vortex formation. The tip leakage vortex is particularly important for noise radiation in this type of turbomachinery. Figure 9 highlights that the tip region noise source relevance is minimal, when compared with the wake sources. This is due to the controlled roll up of the tip vortices.

5. Conclusion

The authors carried out an analysis of the unsteady flow in a large industrial fan designed for one-time-only operation at 400°C. The new design methodology, here under aerodynamic scrutiny, has facilitated development of a range of large fans that complies with the requirements of both EN 12101-3 and ISO 21927-3 during emergency operation.

The authors based their investigation on an Open Source solver, OpenFOAM, using an original very LES sensitized to the backscattering to give an interpretation of the detailed flow topology.

The study of the flow topology was conducted using a vortex eduction criterion based on the pressure Laplacian. The authors found that at the blade hub, a complex vortical pattern takes place as a consequence of the blade section's thickness distribution at the root which induces the formation of a horseshoe vortex system. On the other hand, the tip region features the presence of vortical structures that evolve and interact along the blade stacking line, being generated by the tip leakage vortex swirling core. The analysis of flow field demonstrated that, far from the endwall, the main source of unsteadiness is related to the wake development downstream from the trailing edge.

The quality of the resolved unsteady dynamics of the rotor flow is also indirectly demonstrated by the fair agreement between the prediction and measured sound power spectrum.

Analysis of the Powell sources enables the authors to conclude that the aerodynamic sound generation depends not only on the source term intensity of shear layers, but also the source term fluctuation in both time and spatial domains. Finally it is concluded that vorticity stretching is more relevant than roll up to the generation of aerodynamic sound.

Acknowledgments

References

[1] D. Lacroix, "New french recommendations for fire ventilation in road tunnels," in *Proceedings of the 9th International Conference on Aerodynamics and Ventilation of Vehicle Tunnels*, pp. 103–1123, Aosta Valley, Italy, 1997.

[2] C. Carvel, "The effects of ventilation on fires in tunnels," in *Proceedings of the International Tunnel Fire and Safety Conference*, Rotterdam, The Netherlands, 1999.

[3] A. G. Sheard and N. M. Jones, "Emergency ventilation for vehicular, rail and metro tunnels," in *Proceedings of the International Congress Safety Innovation Criteria inside Tunnels*, Dijon, Spain, 2005.

[4] A. G. Sheard and N. M. Jones, "High temperature certification of large fans for emergency ventilation," in *Proceedings of the 12th International Symposium on Aerodynamics and Ventilation of Vehicle Tunnels*, pp. 123–140, Portoroz, Slovenia, July 2006.

[5] A. G. Sheard and N. M. Jones, "Approval of high-temperature emergency tunnel-ventilation fans: the impact of ISO, 21927-3," in *Proceedings of the ITA–AITES World Tunnel Congress and 34th General Assembly*, Agra, India, 2008.

[6] ANSI/ASHRAE Standard 149-2000, *Laboratory Methods of Testing Fans Used to Exhaust Smoke in Smoke Management Systems*, ANSI/ASHRAE Standard, Atlanta, Ga, USA.

[7] R. A. Wallis, *Axial Flow Fans: Design and Practice*, George Newnes, Lynton, UK, 1961.

[8] B. B. Daily, *Woods Practical Guide to Fan Engineering*, Woods of Colchester, Birmingham, UK, 1985.

[9] J. Vad, "Incorporation of forward blade sweep in the non-free vortex design method of axial flow turbomachinery rotors," *Periodica Polytechnica, Mechanical Engineering*, vol. 45, no. 2, pp. 217–237, 2001.

[10] A. Corsini, F. Rispoli, J. Vad, and F. Bencze, "Non-free vortex flow effects in an axial flow rotor," *Periodica Polytechnica, Mechanical Engineering*, vol. 45, no. 2, pp. 201–216, 2001.

[11] K. Y. Lee, Y. S. Choi, Y. L. Kim, and J. H. Yun, "Design of axial fan using inverse design method," *Journal of Mechanical Science and Technology*, vol. 22, no. 10, pp. 1883–1888, 2008.

[12] J. H. Horlock and J. D. Denton, "A review of some early design practice using computational fluid dynamics and a current perspective," *Journal of Turbomachinery*, vol. 127, no. 1, pp. 5–13, 2005.

[13] M. J. Pratt, "Virtual prototypes and product models in mechanical engineering," in *Proceedings of the IFIP WG 5. 10 Workshop on Virtual Environments and Their Applications and Virtual Prototyping*, pp. 113–128, 1994.

[14] U. Jasnoch, H. Kress, and J. Rix, "Towards a virtual prototyping environment," in *Proceedings of the IFIP WG 5. 10 Workshop on Virtual Environments and Their Applications and Virtual Prototyping*, pp. 173–183, 1994.

[15] A. G. Sheard, A. Corsini, S. Minotti, and F. Sciulli, "The role of computational methods in the development of an aero-acoustic design methodology: application to a family of large industrial fans," CMMF Annual Report, September 2009.

[16] H. Schneider, D. von Terzi, and H. J. Bauer, "Large-Eddy Simulations of trailing-edge cutback film cooling at low blowing ratio," *International Journal of Heat and Fluid Flow*, vol. 31, no. 5, pp. 767–775, 2010.

[17] M. Labois and D. Lakehal, "Very-large eddy simulation (V-LES) of the flow across a tube bundle," *Nuclear Engineering and Design*, vol. 241, pp. 2075–2085, 2011.

[18] L. Davidson and P. Nielsen, "Large eddy simulations of the flow in a three-dimensional ventilated room," in *Proceedings of the 5th International Conference on Air Distribution in Rooms*, pp. 161–168, Yokohama, Japan, 1996.

[19] N. A. Cumpsty, "Review—a critical review of turbomachinery noise," *Journal of Fluids Engineering*, vol. 99, no. 2, pp. 278–293, 1977.

[20] J. H. Miles, "Procedure for separating noise sources in measurements of turbofan engine core noise," in *Proceedings of the 12th AIAA/CEAS Aeroacoustics Conference*, pp. 2249–2264, May 2006.

[21] J. E. Ffowks Williams and D. L. Hawkings, "Sound generation by turbulence and surfaces in arbitrary motion," *Philosophical Transactions of the Royal Society of London A*, vol. 342, 1969.

[22] H. Jasak, "OpenFOAM: a year in review," in *Proceedings of the 5th OpenFOAM Workshop*, Gothenburg, Sweden, June 2010.

[23] D. Borello, A. Corsini, F. Rispoli, and A. G. Sheard, "DES of a large industrial fan at design operation," *Journal of Power and Energy*. In press.

[24] D. Borello, A. Corsini, F. Rispoli, and A. G. Sheard, "LES of the aerodynamics and aero-acoustic performance of an industrial fan designed for tunnel ventilation," ASME Paper GT2012-69046, 2012, submitted to Turbo Expo.

[25] A. Corsini and F. Rispoli, "Flow analyses in a high-pressure axial ventilation fan with a non-linear eddy-viscosity closure," *International Journal of Heat and Fluid Flow*, vol. 26, no. 3, pp. 349–361, 2005.

[26] D. Borello, K. Hanjalic, and F. Rispoli, "Prediction of cascade flows with innovative second-moment closures," *Journal of Fluids Engineering*, vol. 127, no. 6, pp. 1059–1070, 2005.

[27] D. Borello, K. Hanjalic, and F. Rispoli, "Computation of tip-leakage flow in a linear compressor cascade with a second-moment turbulence closure," *International Journal of Heat and Fluid Flow*, vol. 28, no. 4, pp. 587–601, 2007.

[28] D. Borello, G. Delibra, K. Hanjalić, and F. Rispoli, "Large-eddy simulations of tip leakage and secondary flows in an axial compressor cascade using a near-wall turbulence model," *Proceedings of the Institution of Mechanical Engineers A*, vol. 223, no. 6, pp. 645–655, 2009.

[29] D. Borello, G. Delibra, K. Hanjalić, and F. Rispoli, "Hybrid-LES/RANS study of turbulent flow in a low speed linear compressor cascade with moving casing," ASME Paper GT2010-23755, 2010.

[30] G. Delibra, D. Borello, K. Hanjalić, and F. Rispoli, "URANS of flow and endwall heat transfer in a pinned passage relevant to gas-turbine blade cooling," *International Journal of Heat and Fluid Flow*, vol. 30, no. 3, pp. 549–560, 2009.

[31] G. Delibra, D. Borello, K. Hanjalić, and F. Rispoli, "A LES insight into convective mechanism of heat transfer in a wall-bounded pin matrix," in *Proceedings of the 14th International Heat Transfer Conference*, Washington, DC, USA.

[32] M. Lighthill, "On sound generated aerodynamically," *Proceedings of the Royal Society of London A*, vol. 211, 1952.

[33] F. Farassat, "Linear acoustic formulas for calculation of rotating blade noise," *AIAA Journal*, vol. 19, no. 9, pp. 1122–1130, 1981.

[34] S. Bianchi, A. Corsini, and G. Paniagua, "Amplification of the force and tonal noise in transonic HPT," in *Proceedings of the 9th European Turbomachinery Conference*, Istanbul, Turkey, 2011.

[35] Y. Dubief and F. Delcayre, "On coherent-vortex identification in turbulence," *Journal of Turbulence*, vol. 1, pp. 11–22, 2000.

[36] S. Lieblein, "Experimental flow in 2D cascades," in *The Aerodynamic Design of the Axial Flow Compressor*, NACA RME 56B03, reprinted as NASA SP36, Chapter 6, 1956.

[37] D. Borello, A. Corsini, S. Minotti, F. Rispoli, and A. G. Sheard, "U-RANS of a large industrial fan under design and off-design operations," in *Proceedings of the 9th European Turbomachinery Conference*, Istanbul, Turkey, March 2011.

[38] A. Powell, "Theory of vortex sound," *Journal of the Acoustical Society of America*, vol. 36, pp. 177–195, 1964.

[39] N. Curle, "The influence of solid boundaries upon aerodynamic sound," *Proceedings of the Royal Society of London A*, vol. 231, pp. 505–514, 1955.

[40] A. Powell, "Mechanisms of aerodynamic sound production," AGARD Report 466, 1963.

Journal of
Engineering

International Journal of
Rotating
Machinery

The Scientific
World Journal

Journal of
Sensors

International Journal of
Distributed
Sensor Networks

Advances in
Civil Engineering

Journal of
Control Science
and Engineering

Journal of
Robotics

Hindawi

Submit your manuscripts at
http://www.hindawi.com

Journal of
Electrical and Computer
Engineering

Advances in
OptoElectronics

VLSI Design

International Journal of
Navigation and
Observation

Modelling &
Simulation
in Engineering

International Journal of
Aerospace
Engineering

International Journal of
Chemical Engineering

International Journal of
Antennas and
Propagation

Active and Passive
Electronic Components

Shock and Vibration

Advances in
Acoustics and Vibration